

Small Instantons in CP^1 and CP^2 Sigma Models

Yaogang Lian and H. B. Thacker

*Department of Physics, University of Virginia,
P.O. Box 400714 Charlottesville, VA 22901-4714*

(Dated: April 30, 2019)

The anomalous scaling behavior of the topological susceptibility χ_t in two-dimensional CP^{N-1} sigma models for $N \leq 3$ is studied using the overlap Dirac operator construction of the lattice topological charge density. The divergence of χ_t in these models is traced to the presence of small instantons with a radius of order a (= lattice spacing), which are directly observed on the lattice. The observation of these small instantons provides detailed confirmation of Lüscher's argument that such short-distance excitations, with quantized topological charge, should be the dominant topological fluctuations in CP^1 and CP^2 , leading to a divergent topological susceptibility in the continuum limit. For the CP^{N-1} models with $N > 3$ the topological susceptibility is observed to scale properly with the mass gap. These larger N models are not dominated by instantons, but rather by coherent, one-dimensional regions of topological charge which can be interpreted as domain wall or Wilson line excitations and are analogous to D-brane or "Wilson bag" excitations in QCD. In Lorentz gauge, the small instantons and Wilson line excitations can be described, respectively, in terms of poles and cuts of an analytic gauge potential.

I. INTRODUCTION

Recent lattice studies of topological charge structure in pure-gluon QCD have provided evidence that the topological charge density, as constructed from the overlap Dirac operator, organizes into low-dimensional long-range structure [1], consisting of 3-dimensional coherent sheets in 4-dimensional spacetime. A further study demonstrated that this structure is inherently global and that topological charge fluctuations in QCD should be understood not in terms of individual localized lumps but rather as extended brane-like objects [2, 3]. These lattice results challenge the traditional instanton gas or liquid picture [4], in which the QCD vacuum is described as an ensemble of localized (anti-)self-dual lumps of quantized topological charge. On the other hand, the results are quite consistent with the view of QCD theta-dependence provided by string/gauge duality [5] [6], in which topological charge excitations come in the form of membranes or domain walls [7, 8], which are the gauge theory dual of wrapped 6-branes in type IIA string theory. Although the nature of topological charge excitations in QCD is far from a settled issue, lattice studies

may shed light on the dynamics of these coherent fluctuations and their relation to confinement and spontaneous chiral symmetry breaking. Analogous long-range sign-coherent 1-dimensional regions of topological charge density have also been found recently in a Monte Carlo study of 2D CP^{N-1} sigma models [9]. Two-dimensional CP^{N-1} models and four-dimensional QCD have many properties in common. In particular, both are classically scale invariant and have classical instanton solutions of arbitrary radius. Lattice evidence for the existence of long-range coherent structures of codimension one in both QCD and CP^{N-1} strongly supports the understanding of QCD topological charge excitations in terms of membranes. In both of these models it has been argued [9, 10] that the observed membranes are associated with boundaries between “k-vacua”, characterized by an effective local value of θ which jumps by $\pm 2\pi$ across the boundary. The presence of such domain walls in the QCD vacuum was suggested much earlier on the basis of large N chiral symmetry arguments [11]. The same kind of 3D membrane structure in QCD was also identified by Lüscher [12] in the form of “Wilson bags” which are 3-dimensional surface integrals over the 3-index Chern-Simons tensor and are analogous to Wilson lines in the CP^{N-1} models.

In Ref. [9] the scaling behavior of the overlap-based topological susceptibility was studied for CP^1 , CP^3 , and CP^9 . For CP^3 and CP^9 , χ_t was found to scale properly with the mass gap. However, for CP^1 , χ_t exhibits anomalous scaling behavior, giving an apparently divergent topological susceptibility in the continuum limit. This reproduced a result first obtained by Berg and Lüscher in a Monte Carlo study of the lattice $O(3)$ sigma model [13]. The topological susceptibility $\chi_t = \langle Q^2 \rangle / V$ (Q = total topological charge, V = spacetime volume) in two-dimensional CP^{N-1} sigma models would normally be expected to be a renormalization group invariant parameter, which should scale like the squared mass gap μ^2 (μ = mass of nonsinglet meson) for large β ($\beta = 1/g^2$, g is the bare coupling constant). However, the Monte Carlo results reported in Ref. [9] show that χ_t does not even approximately scale in the case of CP^1 , although it does scale properly for CP^3 and CP^9 . Lüscher [14] showed that the anomalous scaling behavior of χ_t for CP^1 could be explained by the contribution of small, point-like instantons with a radius of order a (= lattice spacing). Although the action of a classical continuum instanton is independent of its radius, on the lattice this is not the case, and for CP^1 and CP^2 , the small instantons have such a low action that they overwhelm the contribution of more slowly varying fields which might have been expected to dominate in the continuum limit. This mechanism is at work for CP^1 and CP^2 , but not for CP^3 and higher CP^{N-1} models, because the action of the small instantons is proportional to N and becomes too large to be favored for $N \geq 4$. (As we will show, CP^3 is a marginal case where instantons are observed but do not dominate as in CP^1 and CP^2 .) The abrupt change in

the nature of the dominant topological charge fluctuations as N is increased above 4 provides a detailed Monte Carlo example of the phenomenon first discussed by Witten (for both QCD and CP^{N-1})[11], in which instanton effects are exponentially suppressed at large N , and topological charge is dominated by quantum effects. This can be described, at least figuratively, by saying that instantons “melt” due to quantum fluctuations inherent in the large N_c confining vacuum. For the case of the CP^{N-1} models, the instanton “melting point” is $N \approx 4$.

The definition of the lattice topological charge density used in the original study by Berg and Lüscher was an ultralocal discretization of the topological charge operator in the $O(3)$ sigma model formulation.[13] For our formulation of the lattice CP^{N-1} models, the simplest ultralocal definition of topological charge is the log of the plaquette constructed from the $U(1)$ gauge links,

$$q_p(x) = \frac{1}{2\pi} \text{Im}\{\log[U_\mu(x)U_\nu(x + \hat{\mu})U_\mu^\dagger(x + \hat{\mu} + \hat{\nu})U_\nu^\dagger(x + \hat{\nu})]\} \quad (1)$$

This operator is ultralocal in the gauge fields. It provides an adequate lattice definition of global topological charge and gives results for topological susceptibility which are similar but not identical to those obtained from the overlap formalism. But as a definition of local topological charge density the plaquette-based $q_p(x)$ has severe shortcomings. It suffers from a large amount of short-range noise associated with local gauge field fluctuations, which obscures the long-range coherent topological charge structures found with the overlap-based topological charge density. The overlap definition of the lattice topological charge density is [15]

$$q(x) = \frac{1}{2} \text{tr}[\gamma_5 D(x, x)] \quad (2)$$

where D is a lattice Dirac operator (in our case the overlap operator [16]) which satisfies the Ginsparg-Wilson relation

$$\{D, \gamma_5\} = aD\gamma_5D \quad (3)$$

This construction of the topological charge density on the lattice provides a more incisive probe into the topological structure of gauge field configurations than the plaquette-based operator (1). The exact lattice chiral symmetry of the overlap Dirac operator leads to an implicit “chiral smoothing” of the topological charge which takes place over distances of order a . This reveals the coherent structure of the topological fluctuations without any subjective cooling or smoothing procedure.

In this paper, we investigate the origin of the anomalous scaling behavior of topological susceptibility in two-dimensional CP^1 and CP^2 sigma models, using the overlap construction of the lattice topological charge density. We directly observe small instantons with radii of order a (roughly one

to two lattice spacings) in Monte Carlo configurations for both CP^1 and CP^2 . In the continuum (large β) limit these small instantons dominate the topological susceptibility. In contrast to these point-like small instanton excitations, the topological charge in CP^{N-1} models for $N \geq 4$ has been found to be dominated by one-dimensional line-like “domain wall” structures [9]. After establishing the prevalence of small instantons in CP^1 and CP^2 , we measure the action of an individual small instanton and show that the measured topological susceptibility is in good agreement with a dilute instanton gas calculation. Finally we discuss a description of topological fluctuations in Lorentz gauge which incorporates both small instantons and domain wall structures into a coherent picture in terms of poles and cuts in an analytic gauge potential.

II. ANOMALOUS SCALING BEHAVIOR OF TOPOLOGICAL SUSCEPTIBILITY

A. Lattice CP^{N-1} Sigma Models

The Lagrangian for CP^{N-1} sigma models in the continuum is

$$L = \partial_\mu z_i^* \partial_\mu z_i + (z_i^* \partial_\mu z_i)(z_j^* \partial_\mu z_j) \quad (4)$$

where z^i are N complex fields, $i = 1, \dots, N$, satisfying a constraint $z_i^* z_i = 1$. This Lagrangian is invariant under a local $U(1)$ gauge transformation: $z_i(x) \rightarrow e^{ia(x)} z_i(x)$, for arbitrary space-time dependent $a(x)$. We can introduce a dummy gauge field A_μ and rewrite the Lagrangian as

$$L = (\partial_\mu - iA_\mu) z_i^* (\partial_\mu + iA_\mu) z_i \quad (5)$$

where

$$A_\mu = \frac{1}{2} i(\mathbf{z}^\dagger \partial_\mu \mathbf{z} - (\partial_\mu \mathbf{z})^\dagger \mathbf{z}) \quad (6)$$

To put CP^{N-1} models on the lattice, we introduce $U(1)$ link fields $U(x, x+\hat{\mu}) = e^{iA_\mu(x)}$. CP^{N-1} fields are defined on the sites as $\mathbf{z}(x)$. The lattice action consists of gauge-invariant nearest-neighbor hopping terms,

$$S = \beta N \sum_{x, \hat{\mu}} \mathbf{z}(x)^\dagger U(x, x + \hat{\mu}) \mathbf{z}(x + \hat{\mu}) + c.c. \quad (7)$$

This lattice action is used in our Monte Carlo simulation to generate an ensemble of field configurations. The \mathbf{z} fields are updated by a Cabibbo-Marinari heat bath algorithm, while $U(1)$ link fields are updated by a multi-hit Metropolis algorithm.

B. Overlap Dirac Operator

The overlap Dirac operator [16] preserves exact chiral symmetry on the lattice via the Ginsparg-Wilson relation. For the present work, we employ a standard construction starting from a Wilson-Dirac kernel D_W . The overlap Dirac operator can be written as

$$D = \frac{1}{a}(1 + \gamma_5 \epsilon(H_W(m))) \quad (8)$$

where $H_W(m) = \gamma_5 D_W(-m)$ and

$$\epsilon(H_W(m)) = \frac{H_W(m)}{\sqrt{H_W^\dagger(m)H_W(m)}} \quad (9)$$

It can be easily verified that this construction of the overlap Dirac operator satisfies the Ginsparg-Wilson relation, Eq. (3).

Using the overlap Dirac operator, we can define the lattice topological charge density [15] by Eq. (2), where the trace is summed over spin indices in CP^{N-1} models and over spin and color indices in QCD. The overlap definition of topological charge is not ultralocal in the gauge links. This has the effect of performing some smoothing of the gauge field over a range of order a . For smooth $U(1)$ gauge fields in two dimensions, we find that the overlap topological charge at a site is reasonably well-approximated by the average of the four plaquette-based charges surrounding the site. For a rapidly varying field, and particularly for the small instantons that we observe in CP^1 and CP^2 , the overlap-based charge provides a much clearer view of coherent excitations. The effect of the smoothing obtained by the overlap construction can also be seen in the structure of the 2-point topological charge correlator. Because it is ultralocal, reflection positivity arguments imply that the nearest-neighbor correlator for the plaquette-based charge must be negative. On the other hand, the overlap-based nearest-neighbor correlator is found to be positive. This allows the overlap-based operator to detect sign-coherent structure even if that structure is in the form of small $O(a)$ -radius instantons or membranes of $O(a)$ thickness.

C. Topological Susceptibility

Using the overlap definition of the lattice topological charge density, we have studied the scaling behavior of topological susceptibility χ_t in CP^1 , CP^2 , CP^3 , CP^5 , and CP^9 sigma models. Since χ_t is generally expected to be a renormalization group invariant parameter in two-dimensional CP^{N-1} sigma models, it is expected to scale like a $(mass)^2$ in the continuum limit. There is a

natural mass scale in these models which is the mass gap of the $z_i^* z_j$, ($i \neq j$) meson correlator in the nonsinglet channel. The zero-momentum meson correlator falls off exponentially at large Euclidean time,

$$\int dx_2 \langle z_i^*(x) z_j(x) z_j^*(0) z_i(0) \rangle \sim \text{const.} \times e^{-\mu x_1} \quad (10)$$

where μ is the mass gap.

We have measured the mass gap μ in lattice units for various values of N and β as shown in Table I. We worked on lattice sizes up to 100×100 . For each N , β has been chosen to cover the

TABLE I: Mass gap of the meson correlator in lattice units

β	CP^1	β	CP^2	β	CP^3	β	CP^5	β	CP^9
1.0	.438(5)	0.9	.436(5)	0.8	.554(2)	0.7	.652(6)	0.7	.406(2)
1.1	.286(5)	1.0	.275(2)	0.9	.327(3)	0.8	.360(3)	0.8	.212(2)
1.2	.179(3)	1.1	.155(1)	1.0	.180(1)	0.9	.186(3)	0.9	.0895(6)
1.3	.111(1)	1.2	.084(2)	1.1	.088(1)	1.0	.085(1)	1.0	.0579(2)
1.4	.070(1)	1.3	.043(1)	1.2	.0531(3)	1.1	.0496(9)	1.1	.0475(4)
1.5	.036(1)	1.4	.0256(8)	1.3	.0264(7)	1.2	.0308(4)	1.2	.0287(4)
1.6	.0238(8)	1.5	.0207(5)	1.4	.0217(5)	1.3	.0249(2)	1.3	.0255(3)

region where correlation length $\xi = 1/\mu$ varies from roughly 3 to 50. For each set of N and β , the meson correlator was averaged over 4000 field configurations. The correlator fits were carried out by a standard covariant χ^2 minimization.

The topological susceptibility χ_t can be determined from the large- V limit of

$$\chi_t^{(V)} = \langle Q^2 \rangle / V \quad (11)$$

where Q is the total topological charge on the lattice and V is the space-time volume. An equivalent way to measure χ_t is to integrate the two-point topological charge density correlator,

$$\chi_t = \sum_x \langle q(x) q(0) \rangle \quad (12)$$

where $q(x)$ is calculated from the overlap definition (Eq. 2). If the correlator calculation is carried out at finite volume, and the integral is taken over the entire volume of the lattice, this gives results identical to those obtained by measuring the global charge Q of each configuration and using (11). However, we have found that at large values of β , where the correlation length μ^{-1} is long and finite

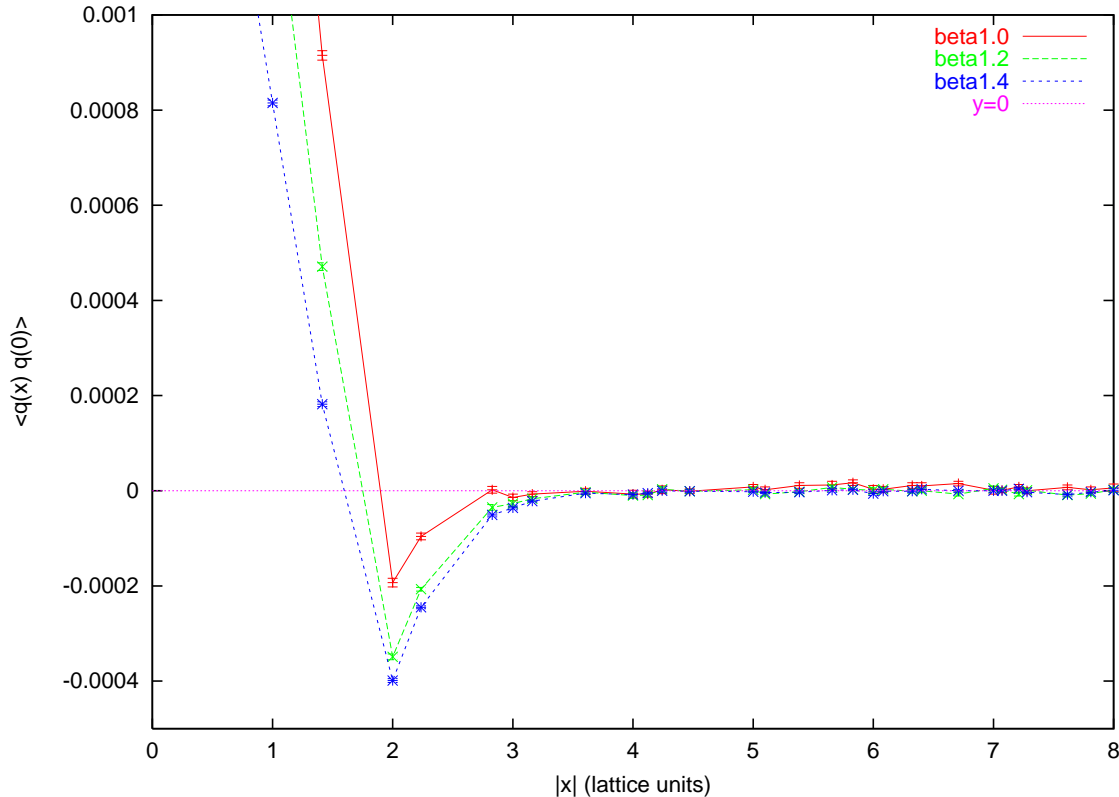


FIG. 1: The two-point topological charge density correlator for CP^1 with several values of β .

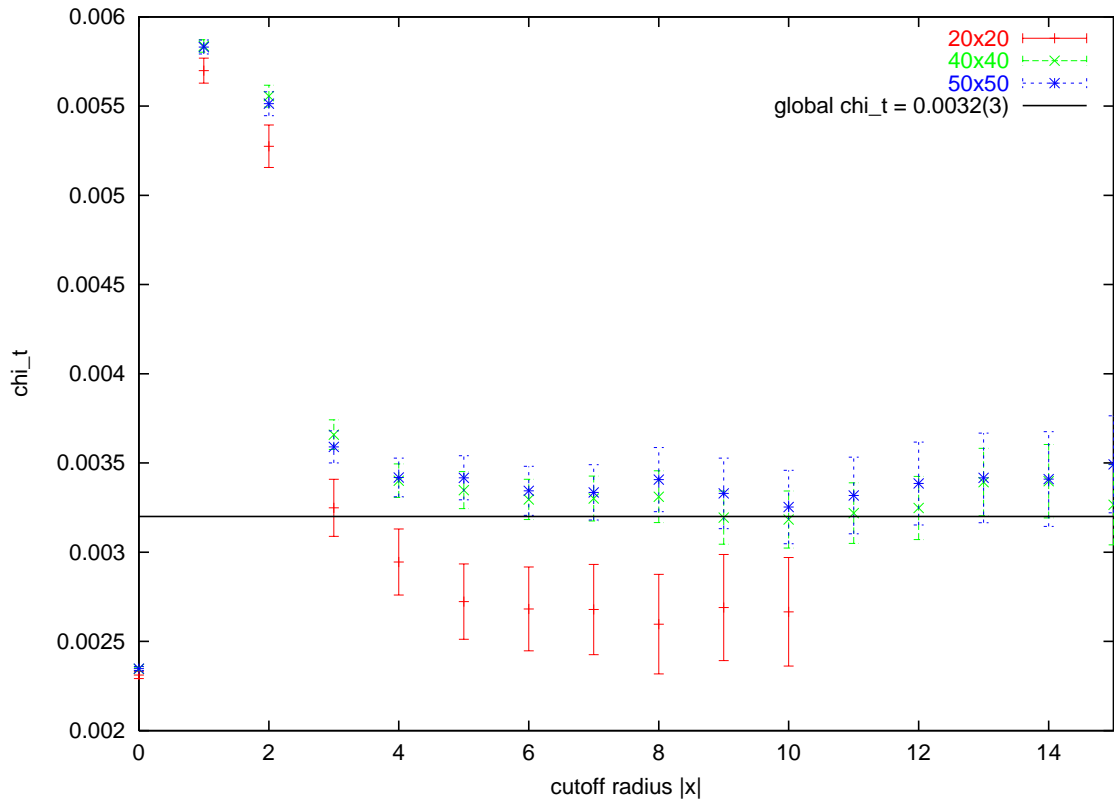
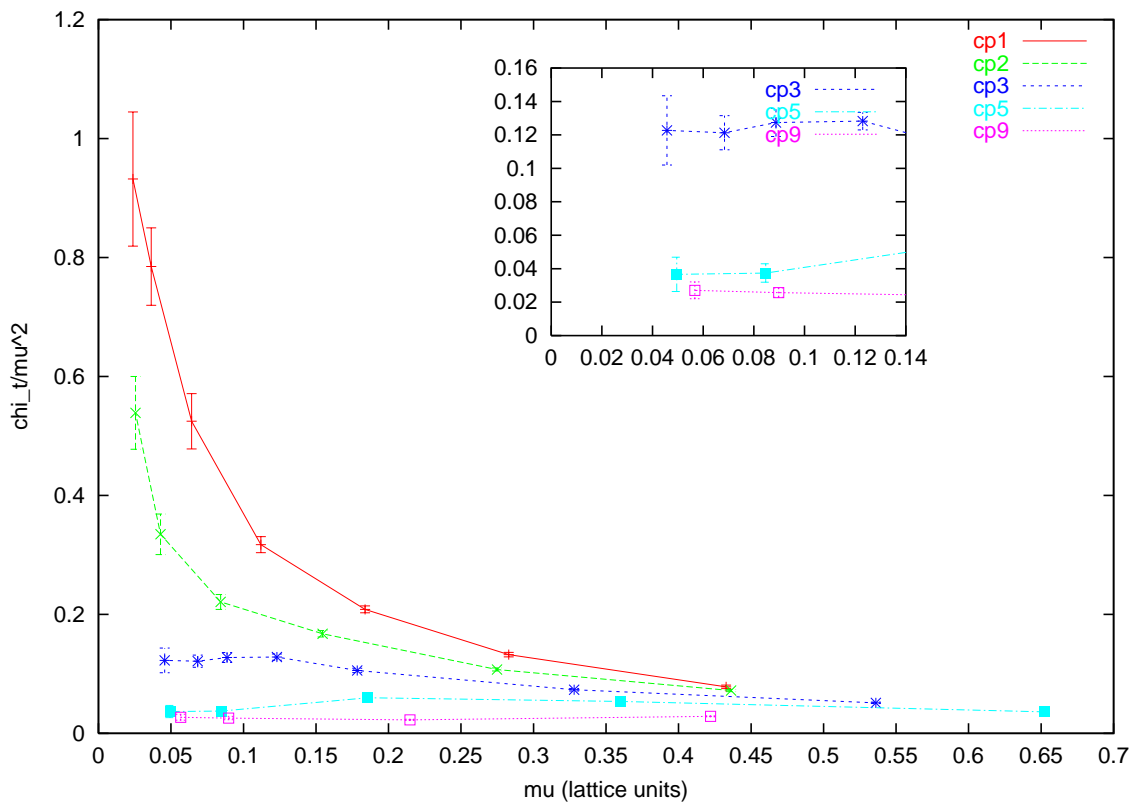
volume effects become important, a method based on a truncated integration of the correlator is much less affected by finite volume corrections than the calculation based on measurement of the global charge Q . The infinite volume topological charge correlator is very short range, consisting of a positive core at $x < 2$ and a short-range negative tail which falls off rapidly, even when the nonsinglet meson correlation length μ^{-1} is quite long. Fig. 1 shows the point-to-point correlator $\langle q(x)q(0) \rangle$ for CP^1 for several different values of β . Over this same range, μ^{-1} varies from 2.3 to 14.4. For larger values of β , where the correlation length becomes comparable to the box size, the global charge Q freezes to zero. The integrated correlator also goes to zero, but, at least for correlation lengths up to about half the box size, the shape and magnitude of the short-range topological charge correlator remains relatively unchanged from its infinite volume value. The fact that the integrated finite volume correlator is smaller comes about through a cancellation between the short range part of the integral (which still gives a reasonable approximation to the infinite volume susceptibility) and a negative background contribution which does not fall off as rapidly with distance and therefore gets most of its contribution from larger $|x|$. By comparing the correlator on several box sizes, we find that this longer range negative background is a finite volume effect. As a result, on smaller boxes the integrated short-range correlator gives a better estimate

of the infinite volume χ_t than one could obtain from the fluctuations of the global charge. After experimenting with different prescriptions for cutting off the short-range correlator integration, we have chosen to calculate the correlator as a function of $|x|$ and integrate out to a cutoff value of $|x| \leq x_c$ for which the measured correlator is within one standard deviation of zero. This was always in the range $3 < x_c < 5$. Results were essentially unchanged if we used a constant cutoff of $x_c = 4$. To test the method, we calculated χ_t as a function of the cutoff radius for CP^3 at $\beta = 1.0$ on various lattice sizes, as shown in Fig. 2. χ_t measured on the 40×40 lattice matches nicely with that measured on the 50×50 lattice at each cutoff radius. This shows that the 50×50 lattice is large enough to give a correct χ_t that is close to the infinite volume susceptibility. By using (11) on the 50×50 lattice configurations, we obtained $\chi_t = 0.0032(3)$. From the graph, we observe that χ_t measured on the 40×40 or 50×50 lattice quickly converges to the infinite volume result when $x_c \approx 4$. However, on the 20×20 lattice, χ_t converges to a value lower than the infinite volume result. On the other hand, if we apply the cutoff at $x_c \approx 4$, we can still extract approximately the right value of χ_t on the 20×20 lattice. Most of the finite volume effect that causes the globally determined χ_t to be too small on the 20×20 lattice comes from distances > 4 . On the larger 40×40 and 50×50 lattices, the value obtained for χ_t is essentially independent of the cutoff for $x_c > 4$, indicating that the longer range negative contribution from $|x| > 4$ on the smaller box is a finite volume effect. This shows that the truncated integration method is less affected by finite volume than a calculation based on measurement of the global charge Q . Using the truncated integration method, we have measured χ_t in lattice units for various values of N and β , as shown in Table II.

TABLE II: Topological susceptibility χ_t in lattice units

β	CP^1	β	CP^2	β	CP^3	β	CP^5	β	CP^9
1.0	.0146(2)	0.9	.0137(2)	0.8	.0147(2)	0.7	.0154(3)	0.7	.0051(1)
1.1	.0106(2)	1.0	.0081(2)	0.9	.0079(2)	0.8	.0069(1)	0.8	.00105(5)
1.2	.0070(2)	1.1	.0040(1)	1.0	.0034(1)	0.9	.0021(1)	0.9	.00021(2)
1.3	.0040(1)	1.2	.00157(7)	1.05	.00194(8)	1.0	.00027(4)	1.0	.00009(2)
1.4	.0022(1)	1.3	.00056(5)	1.1	.00100(6)	1.1	N/A	1.1	N/A
1.5	.00104(5)	1.4	.00035(3)	1.15	.00057(5)	1.2	N/A	1.2	N/A
1.6	.00053(5)	1.5	N/A	1.2	.00026(4)	1.3	N/A	1.3	N/A

To show the scaling behavior of χ_t with respect to $(mass)^2$, we plot χ_t/μ^2 vs. μ in Fig. 3. A constant value on the graph indicates proper scaling. From the graph we observe that χ_t appears to scale properly for CP^3 , CP^5 , and CP^9 in the continuum limit, but it does not even approximately

FIG. 2: χ_t vs. cutoff radiusFIG. 3: Scaling behavior of χ_t/μ^2 in CP^1 , CP^2 , CP^3 , CP^5 and CP^9

scale for CP^1 and CP^2 . Our results confirm that the overlap-based χ_t exhibits the same anomalous scaling behavior observed in the $O(3)$ sigma model formulation of CP^1 [13]. From Fig. 3 we see that this anomalous scaling behavior occurs in CP^1 and CP^2 , but not in CP^3 , CP^5 , or CP^9 . This is exactly the behavior predicted by Lüscher [14], who showed that, for $N \leq 3$, the topological susceptibility should be dominated by small instantons with a radius of order a . In the next section, we will discuss the theoretical explanation of the anomalous scaling behavior of χ_t , present the direct observation of small instantons in Monte Carlo configurations, and discuss some properties of these objects.

III. SMALL INSTANTONS

The divergent behavior of χ_t in CP^1 and CP^2 can be attributed to instantons with a radius of approximately one to two lattice spacings. These small instantons are short-range gauge field fluctuations with quantized topological charge. In the space of lattice gauge field configurations they reside near the boundary between the $Q = 1$ and $Q = 0$ sectors, in the sense that a small adjustment of the gauge links will cause the instanton to “fall through the lattice” and turn into a $Q = 0$ configuration. The dominance of these small instanton configurations violates the usual assumptions about the continuum limit. In a naive view of the continuum limit, one would assume that configurations are dominated by fields for which the values of gauge-invariant local densities (e.g. action density or topological charge density) are smooth over distances of order a . Although the probability for the small instantons to occur is exponentially small, the probability for more smoothly varying fields to have nonzero total topological charge is also exponentially small. Which type of fluctuation dominates the topological susceptibility depends on the precise value of the instanton action.

If we only take into account the contribution from the slowly varying fields, the topological susceptibility should scale like a $(mass)^2$ in the continuum limit, i.e.

$$\chi_t^{s.v.} \propto \beta^{4/N} e^{-4\pi\beta}, \quad (\beta \rightarrow \infty) \quad (13)$$

However, if we take into account the contribution from small instantons, a dilute gas calculation yields

$$\chi_t^{d.g.} \propto \beta^{-1} e^{-\beta\epsilon}, \quad (\beta \rightarrow \infty) \quad (14)$$

where $\beta\epsilon$ is the minimal action of gauge field configurations in the $Q = 1$ sector.

In Ref. [14] the minimum-action field configuration with $Q = 1$ was constructed and its action was calculated. This gave the value of ϵ in the $O(3)$ model as $\epsilon = 6.69\dots$. For other CP^{N-1} models, it was argued that the minimal action of a small instanton should be proportional to N , according to the inherent factor of N in the CP^{N-1} action (see Eq. 7). Since $\epsilon < 4\pi$ for CP^1 and CP^2 , the small instantons make the dominant contribution to the topological susceptibility. This explains why χ_t does not scale as μ^2 in the continuum limit in CP^1 and CP^2 . However, for CP^{N-1} models with $N > 3$, $\epsilon = \frac{N}{2} \cdot 6.69 > 4\pi$, so χ_t is dominated by less singular topological fluctuations. On the other hand, even for $N > 3$, the dominant excitations are not smooth distributions of topological charge, but rather, singular domain-wall type excitations which give rise to a dominant contact term in the 2-point correlator [9].

Even a qualitative survey of overlap topological charge distributions in the Monte Carlo configurations is sufficient to identify small instantons as the origin of the divergence of χ_t in CP^1 and CP^2 . To emphasize this point, we will first present a few typical configurations. Small instantons are particularly prominent and easy to identify at large values of β , where the meson correlation length μ^{-1} is large. Interestingly, the finite volume effects on the fluctuation of the global topological charge Q are completely different for CP^1 and CP^2 than they are for the $N \geq 4$ models. For CP^3 and higher, the fluctuation of Q to nonzero integer values “freezes out” at large values of β for a lattice with a fixed number of sites. When the correlation length becomes comparable to the box size, Q stops fluctuating altogether. In marked contrast, for example, CP^1 on a 40x40 lattice continues to fluctuate to nonzero Q well above $\beta = 1.6$, where the correlation length μ^{-1} is greater than 40. This is apparently due to the fact that the small instantons remain of order lattice spacing in size, even when the correlation length becomes large. They are therefore not very susceptible to being squeezed out by finite volume effects at the scale of the correlation length. In Fig. 4 we show several typical configurations. Fig. 4(a) is a CP^1 configuration with $\beta = 2.5$ and $Q = 1.0$. It clearly shows a positively charged peak which is distinctly different from the background quantum fluctuations. We will refer to these objects, which are easily identified in the large β regime, as “peak structures.” As we discuss below, the amount of charge contained in a typical peak structure is approximately one unit, so they clearly exhibit local quantization of topological charge. Furthermore, for large values of β , fluctuations of the global charge Q by a unit during the Monte Carlo run are always accompanied by the appearance or disappearance of one of these peak structures. For comparison, we also show a CP^1 configuration with $\beta = 2.5$ and $Q = 0$ in Fig. 4(b), where no peak structure can be seen. Fig. 4(c) shows two negative peak structures in a CP^1 configuration with $\beta = 1.6$ and $Q = -2.0$. Because of the smaller value of β ,

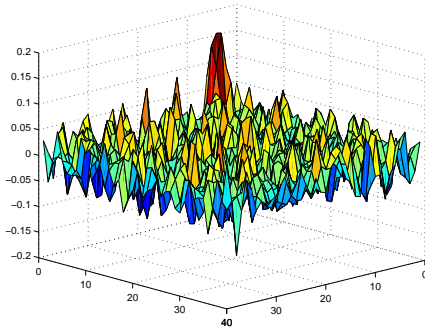
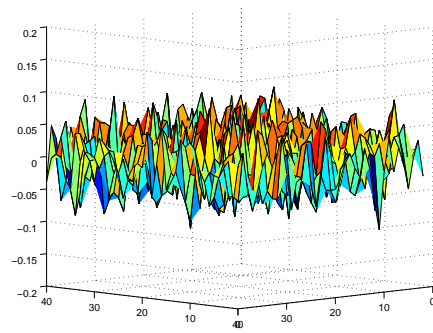
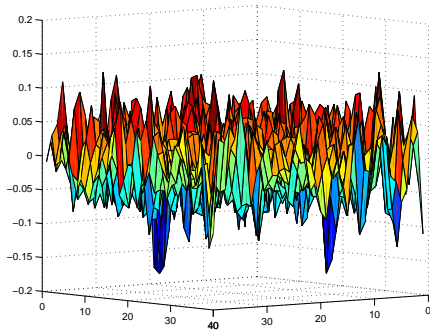
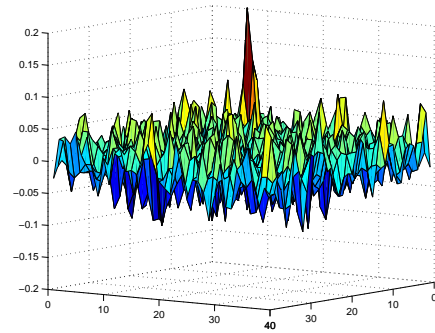
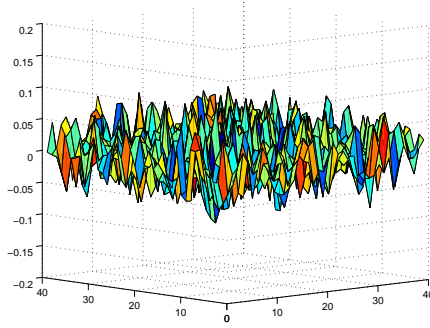
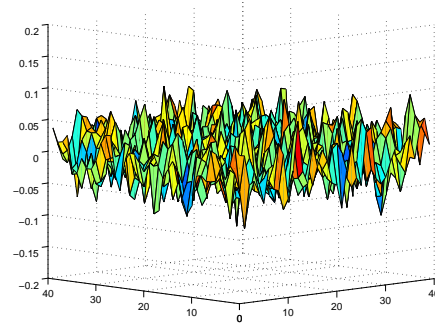
(a) CP^1 , $\beta = 2.5$, $Q = 1.0$ (b) CP^1 , $\beta = 2.5$, $Q = 0$ (c) CP^1 , $\beta = 1.6$, $Q = -2.0$ (d) CP^2 , $\beta = 1.8$, $Q = 1.0$ (e) CP^3 , $\beta = 1.6$, $Q = 0$ (f) CP^9 , $\beta = 0.9$, $Q = -1.0$

FIG. 4: (a) A peak structure is clearly seen in a CP^1 configuration with $\beta = 2.5$ and $Q = 1.0$. (b) No peak structures in CP^1 with $\beta = 2.5$ and $Q = 0$. (c) Two negative peak structures in CP^1 with $\beta = 1.6$ and $Q = -2.0$. (d) A peak structure in CP^2 with $\beta = 1.8$ and $Q = 1.0$. (e) CP^3 with $\beta = 1.6$ and $Q = 0$ shows no peak structure. (f) CP^9 with $\beta = 0.9$ and $Q = -1.0$ shows no peak structure.

the background quantum fluctuations are seen to be larger than in the previous plots. The CP^2 configuration in Fig. 4(d) also shows a peak structure with $\beta = 1.8$ and $Q = 1.0$. However, at comparable correlation lengths, the CP^3 and CP^9 configurations contain no prominent peaks and always have zero total topological charge on a 40×40 lattice. Fig. 4(e) shows a CP^3 configuration with $\beta = 1.6$ and $Q = 0$, where no peak structure can be seen. Finally, Fig. 4(f) shows a CP^9 configuration with $\beta = 0.9$ and $Q = -1.0$. Here, in spite of the fact that Q is nonzero, there is no sign of an integer charged peak structure. In fact, for CP^5 and CP^9 , there were no integer charged peak structures in any of the configurations studied. The case of CP^3 is interesting because, although there is some indication of small instantons (see below), they are not as dominant as in CP^1 and CP^2 . Note that the one-instanton action of $\epsilon = 14.1$ for CP^3 is slightly above the instanton “melting point” of $4\pi = 12.57\dots$ predicted in the dilute gas approximation. In the case of CP^3 , the small instantons do not lead to any observable anomalous scaling of χ_t because their action is very close to 4π .

To add further support for the assertion that the peak structures in CP^1 and CP^2 are indeed small instantons, we measured the topological charge inside the highest peak structure in each field configuration. As we will show in the following discussion, a good effective definition of the topological charge within a peak is given by the sum of the charges within a radius ≤ 2 of the maximum-charge site. To illustrate the quantization of the charge in the peak structures, we analyze, for several values of β and N , a large sample of configurations which have a global topological charge of $Q = \pm 1$. For each configuration we calculate the amount of charge within the highest peak structure. The histograms show the number of configurations which have a charge within a given range for the highest structure. As clearly shown, the CP^5 and CP^9 models exhibit very different histograms from CP^1 , CP^2 and CP^3 . The CP^5 and CP^9 configurations typically have much less than a unit of topological charge in the highest peak structure, while in CP^1 , CP^2 and CP^3 , the majority of $Q = \pm 1$ configurations have a structure which contains approximately a unit of topological charge. This clearly confirms that the peak structures we observed in Fig. 4 are in fact small instantons with a radius of < 2 lattice spacings. By contrast, the topological structures in higher CP^{N-1} models exhibit no tendency toward local quantization, consistent with expectations from the domain-wall picture of topological charge excitations in these models.

To estimate the approximate radial size of the peak structures, we considered an ensemble of CP^1 configurations on a 40×40 lattice at $\beta = 1.8$, where we have 72 $Q = \pm 1$ configurations out of 400. In each configuration, we started with the highest peak, then measured the topological charge density $q(r)$ and the integrated topological charge $Q(r)$ within radius r . Fig. 6(a) shows

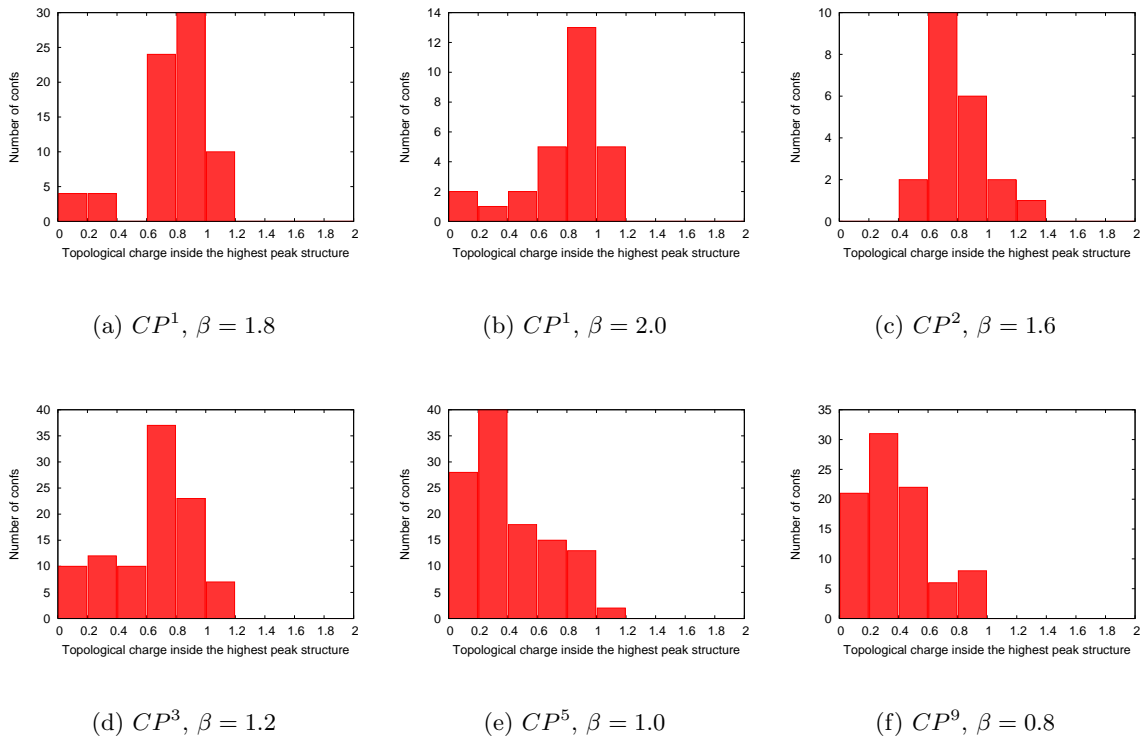


FIG. 5: Histogram of the number of configurations with respect to the topological charge inside the highest peak structure

the r dependence of $q(r)$ and $Q(r)$ with error bars. We see from the graph that $q(r)$ drops to zero at about $r \approx 2$, while at the same time $Q(r)$ goes up to ≈ 1.0 . For this reason, we define the peak structure as occupying the lattice sites within a radius of two lattice spacings from the peak. We also observe from the graph that the $q(r)$ fluctuates around zero when $r > 2.0$ and the fluctuation is comparable to error bars. This confirms that the radial size of the peak structures we observed in Fig. 4 is indeed roughly 1 to 2 lattice spacings. All of these properties fit precisely the description of small instantons, which arise on the lattice as minimum action configurations in the $Q = \pm 1$ sector.

In order to compare topological susceptibility measurements with the predictions of a dilute gas of small instantons, we want to determine the action of a single small instanton by measuring the minimal action in the $Q = 1$ sector for various CP^{N-1} models. The value of the minimal action for a small instanton determines whether they will dominate the topological fluctuations in the continuum limit. For CP^1 and CP^2 the value of the minimal action also determines the form of the divergence of χ_t in the continuum limit. We constructed a small instanton configuration on the lattice, which consists of three vertical links of $e^{i\eta}$, $e^{i\pi}$, and $e^{-i\eta}$ respectively on three adjacent

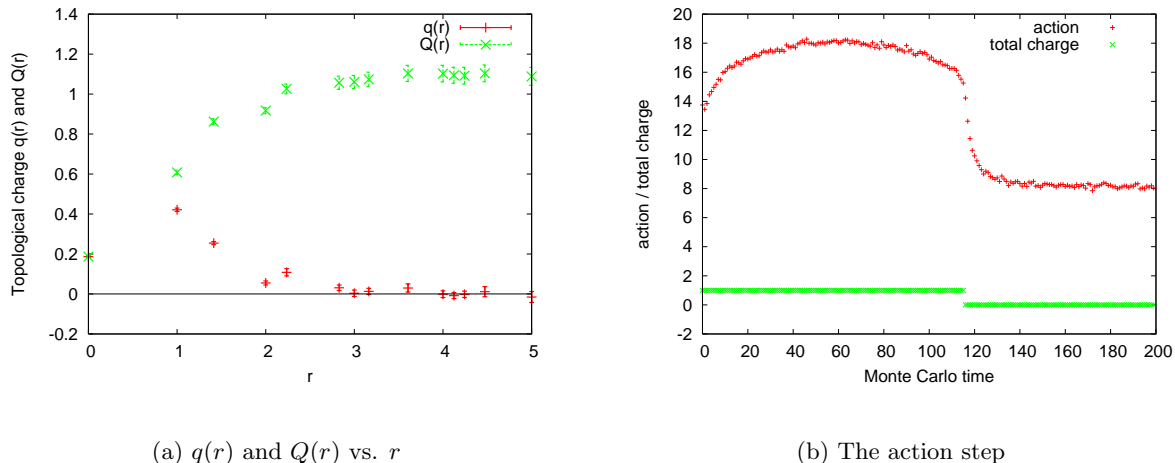


FIG. 6: (a) The r dependence of the topological charge density $q(r)$ and the total topological charge $Q(r)$ within radius r ; (b) The gauge field action steps down when the CP^1 configuration tunnels from $Q = 1$ into $Q = 0$ sector. The upper curve is the action and the lower curve is the charge Q .

sites on a horizontal row, while all other links are set to one. Here the value of η is taken at the boundary between the $Q = 1$ and $Q = 0$ sectors, as determined by the overlap Q . This gives, $\eta = .0873(1)$. We then annealed this configuration (by running the Monte Carlo on the z fields at large β with fixed gauge links) and measured its action. The minimal actions we obtained are: $\epsilon = 6.76$ for CP^1 , $\epsilon = 10.41$ for CP^2 and $\epsilon = 14.08$ for CP^3 . For CP^1 this is close to Lüscher's result $\epsilon = 6.69$ [14]. Since our lattice action and definition of topological charge differ from the $O(3)$ model formulation, exact agreement between our measured ϵ and that of Ref.[14] is not expected. We also looked at how the lattice action changes when we let a CP^1 configuration tunnel from the $Q = 1$ sector into the $Q = 0$ sector, starting with a Monte Carlo generated $Q = 1$ configuration and cooling it by running at a very large β . An action step is expected which should be close to the minimal action in the $Q = 1$ sector. Fig. 6(b) clearly shows the action step when the tunneling occurs. The action step is measured to be about 7, which is very close to the one-instanton action.

Some insight into the dynamics of small instantons in CP^1 and CP^2 can be obtained by comparing the measured topological susceptibility with the prediction of a dilute instanton gas calculation. In the dilute gas approximation, the topological susceptibility is determined by the one-instanton action ϵ , and behaves like

$$\chi_t^{d.g.} \propto \beta^{-1} e^{-\beta\epsilon}, \quad (\beta \rightarrow \infty) \quad (15)$$

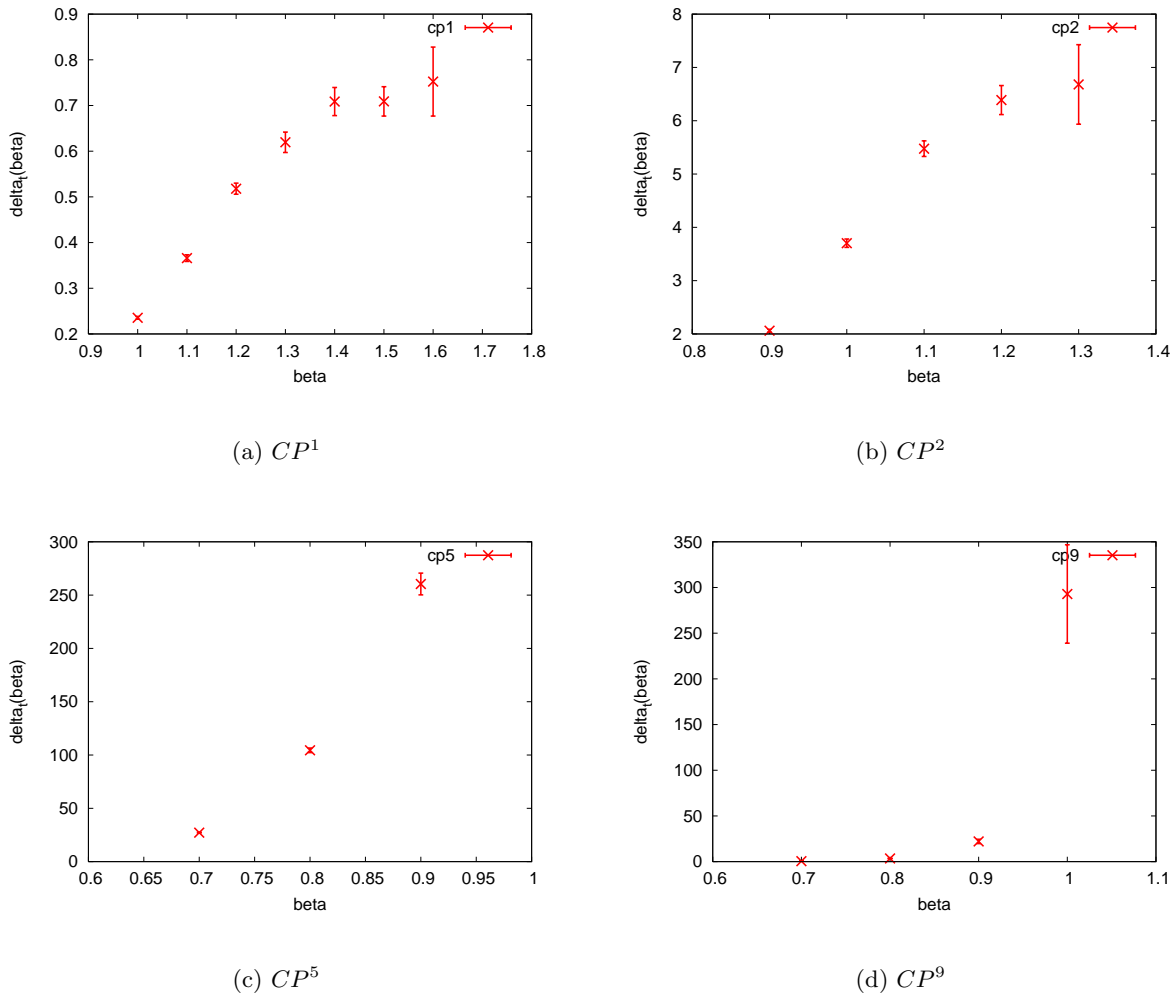


FIG. 7: Plot of the coefficient $\delta_t(\beta)$ defined in Eqn. 16.

To test how well the dilute gas approximation works, we plot the quantity

$$\delta_t(\beta) = \beta e^{\beta\epsilon} \chi_t(\beta) \quad (16)$$

against β in Fig. 7, up to an irrelevant overall factor. Fig. 7(a) and 7(b) show that δ_t becomes roughly constant at large β for CP^1 and CP^2 , confirming the dilute gas calculation. However, δ_t is a rapidly increasing function of β for CP^5 and CP^9 , showing that the expected contribution from instantons (15) is much smaller than the measured topological susceptibility. This confirms the conclusion that small instantons are irrelevant to the determination of χ_t for $N > 4$.

In the next section we discuss the mechanism of topological charge fluctuations in different CP^{N-1} models. We will argue that small instantons and membrane structures are the two types of lower dimensional topological structures (zero- and one-dimensional respectively) that can appear

in CP^{N-1} models.

IV. MECHANISM OF TOPOLOGICAL CHARGE FLUCTUATIONS

As we have shown in the previous section, small instantons dominate topological charge fluctuations in CP^1 and CP^2 and produce anomalous scaling behavior of χ_t , while CP^3 and higher CP^{N-1} models exhibit proper scaling behavior $\chi_t \sim \mu^2$. Thus, in the continuum limit, CP^1 and CP^2 have infinite topological susceptibility. The original observation of this divergent susceptibility [13] was obtained with an ultralocal definition of topological charge in the $O(3)$ sigma model formulation. The fact that the same divergent behavior of χ_t/μ^2 occurs when one uses the overlap construction suggests that the divergence cannot be eliminated by a better lattice definition of topological charge, and that it has some physical significance in the continuum limit. To gain a better understanding of this, it is useful to consider the topological charge correlator in Euclidean 2-space,

$$G(x) = \langle q(x)q(0) \rangle \quad (17)$$

The lattice studies discussed here and in Ref. [9] provide clear evidence that, in the continuum limit, this correlator is very short range (compared to the correlation length μ^{-1}), so one might expect an operator product expansion to provide insight. Here we consider an operator product expansion in the effective $U(1)$ gauge theory obtained by integrating out the z -fields. Taking the large N solution as a guide, we expect that the charged z -particles acquire a “constituent quark mass” M . At the same time, z -loop effects produce a dynamically generated kinetic $F_{\mu\nu}^2$ term in the effective gauge action. This effect leads to a confining Coulomb potential between constituent z -particles. However, in the large N limit, the confining potential is weak, corresponding to a string tension of order M^2/N . Thus, one can distinguish between a relatively long distance scale $\sim \sqrt{N}M^{-1}$ associated with confinement, and a shorter distance scale of order M^{-1} , which probes the substructure of the constituent z particles. By invoking the operator product expansion in the effective gauge theory obtained by integrating out the z -fields, we are assuming that the distance scales relevant to topological structure are characterized by the confinement scale. The large N solution, discussed below, provides a good illustration of the order of limits involved here. In the large N approximation, after integrating out the z fields, the action $L(x)$ can be replaced by

$$L(x) \rightarrow \frac{1}{4}F_{\mu\nu}^2 \quad (18)$$

where $F_{\mu\nu}$ is a rescaled field strength obtained by the replacement

$$A_\mu \rightarrow \sqrt{\frac{12\pi M^2}{N}} A_\mu \quad (19)$$

The two lowest dimension gauge invariant, Lorentz invariant local operators that can appear in the OPE for (17) are the identity and the squared field strength $F_{\mu\nu}^2 \equiv F^2$,

$$q(x)q(0) \sim C_1(x) + C_2(x)F^2(0) + \dots \quad (20)$$

where \dots represents operators of dimension greater than 2. In the following discussion, it will also be useful to consider the corresponding OPE coefficients for the product of two Chern-Simons currents. Defining

$$J_\mu^{CS}(x) = \frac{1}{2\pi} \epsilon_{\mu\nu} A_\nu(x) \quad (21)$$

we write the OPE (ignoring possible gauge-dependent terms which do not contribute to (20)),

$$J_\mu^{CS}(x)J_\nu^{CS}(0) \sim C_{1\mu\nu}(x) + C_{2\mu\nu}(x)F^2(0) + \dots \quad (22)$$

The Chern-Simons correlator

$$G_{\mu\nu}^{CS}(x) = \langle J_\mu^{CS}(x)J_\nu^{CS}(0) \rangle \quad (23)$$

is related to the topological charge correlator (17) by

$$G(x) = -\partial_\mu \partial_\nu G_{\mu\nu}^{CS}(x) \quad (24)$$

In the free theory defined by (18), the behavior of the OPE coefficients is given by naive dimensional counting. For the topological charge OPE, this would give.

$$C_1(x) \sim 1/x^4 \quad (25)$$

$$C_2(x) \sim 1/x^2 \quad (26)$$

However, we will see in the following discussion that, although such power-law behavior is true in the OPE for the Chern-Simons correlator, the corresponding OPE for the topological charge correlator “collapses” to pure contact terms of the form

$$C_1(x) \sim \nabla^2 \delta^2(x) \quad (27)$$

$$C_2(x) \sim \delta^2(x) \quad (28)$$

As we argue below, this collapsing of the operator product expansion for $G(x)$ is a consequence of the lower dimensional character of the small instanton and domain wall excitations of topological charge. The Fourier transformed OPE coefficients

$$\tilde{C}_i(q) = \int d^2x C_i(x) e^{iq \cdot x} \quad (29)$$

have large q^2 behavior

$$\tilde{C}_1(q^2) \sim q^2 \quad (30)$$

$$\tilde{C}_2(q^2) \sim 1 \quad (31)$$

The singular terms in the operator product expansion correspond to polynomial subtraction terms in the dispersion integral representation of the two-point correlator. We consider the correlator in momentum space,

$$\tilde{G}(q^2) = \int d^2x e^{iq \cdot x} G(x) \quad (32)$$

Under general assumptions, the correlator can be written in a dispersion integral representation [17, 18],

$$\tilde{G}(q^2) = c_1 q^2 + c_2 - \int_{M_0^2}^{\infty} d\lambda^2 \frac{\rho(\lambda^2)}{q^2 + \lambda^2} \quad (33)$$

(Note: This representation holds in two space-time dimensions. In four dimensions, the polynomial part can include a q^4 term.) The first two terms represent contact terms associated with the short distance singularities of the OPE (20). The integral term represents the contribution of real intermediate states of invariant mass λ . Here M_0 is the mass gap in the flavor singlet channel. The standard way of analyzing correlators on the lattice is to pick a time direction and Fourier transform over the spatial direction with spatial momentum component $q_1 = 0$, i.e.

$$\hat{G}(t) = \int dx_1 G(x_0 = t, x_1) \quad (34)$$

The dispersion representation then gives

$$\hat{G}(t) = -c_1 \delta''(t) + c_2 \delta(t) - \int_{M_0^2}^{\infty} \frac{d\lambda^2}{2\lambda} \rho(\lambda^2) e^{-\lambda|t|} \quad (35)$$

The topological susceptibility is

$$\chi_t = c_2 - \int_{M_0^2}^{\infty} \frac{d\lambda^2}{\lambda^2} \rho(\lambda^2) \quad (36)$$

Note that the c_1 contact term arises from the identity operator term in the OPE, while the c_2 term arises from the F^2 insertion term. The c_1 term does not contribute to χ_t and the c_2 term must be positive and larger in magnitude than the negative contribution from the integral over real intermediate states in order for χ_t to be positive.

A detailed numerical analysis of the spectral and scaling properties of the $q(x)$ correlator will be reported elsewhere. Here we will quote and utilize some of the main properties of the correlator which emerge from this numerical study. The results are found to be consistent with the assumption that the correlator is reasonably well-described by contact terms alone, without the need for an intermediate state term. We should emphasize that a description of the correlator as purely contact terms does not mean that real propagating intermediate states do not contribute, but only that those states are heavy compared to the q^2 values we are probing on the lattice when we calculate the two-point correlator. The effect of heavy intermediate states can be absorbed into the contact terms via

$$c_1 \rightarrow c_1 + \int_{M_0^2}^{\infty} \frac{d\lambda^2}{\lambda^4} \rho(\lambda^2) \quad (37)$$

$$c_2 \rightarrow c_2 - \int_{M_0^2}^{\infty} \frac{d\lambda^2}{\lambda^2} \rho(\lambda^2) \quad (38)$$

The large N solution [11, 19] provides an explicit example which illustrates how the pure contact term approximation to G arises. We consider the gauge field vacuum polarization tensor (the inverse of the $\langle A_\mu A_\nu \rangle$ correlator) in momentum space,

$$\Delta_{\mu\nu}^{-1} \equiv \left(\delta_{\mu\nu} - \frac{q_\mu q_\nu}{q^2} \right) (\Delta(q^2))^{-1} \quad (39)$$

Since $2\pi q(x)$ is just the curl of A_μ ,

$$q(x) = \frac{1}{2\pi} \epsilon_{\mu\nu} \partial_\mu A_\nu \quad (40)$$

the gauge correlator is related to the topological charge correlator by

$$4\pi^2 \tilde{G}_{\mu\nu}^{CS}(q) = \frac{q_\mu q_\nu}{q^2} \Delta(q^2) \quad (41)$$

or

$$4\pi^2 \tilde{G}(q^2) = q^2 \Delta(q^2) \quad (42)$$

In the large N limit, this is determined by a one loop calculation depicted in Fig. 8, which gives

$$\Delta(q^2) = \frac{2\pi}{N} \left[\xi(q^2) \ln \left(\frac{\xi(q^2) + 1}{\xi(q^2) - 1} \right) - 2 \right]^{-1} \quad (43)$$

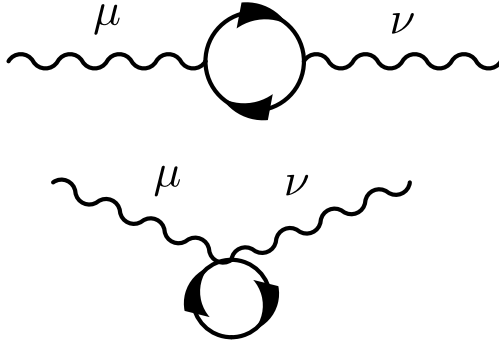


FIG. 8: One-loop graphs contributing to the gauge field correlator in the large N approximation.

where $\xi(q^2) = \sqrt{1 + \frac{4M^2}{q^2}}$. In this example, the pure contact term approximation to the topological charge correlator is obtained by assuming that the mass gap $M_0 = 2M$ is large compared to the momenta relevant to topological charge structure, i.e. $4M^2 \gg q^2$. Expanding in powers of q^2/M^2 and neglecting terms that vanish in the limit $q^2/M^2 \rightarrow 0$, we get

$$\Delta(q^2) = \frac{12\pi M^2}{Nq^2} + \frac{6\pi}{5N} + O\left(\frac{q^2}{M^2}\right) \quad (44)$$

Note the presence of a $q^2 = 0$ pole in the gauge field correlator. Since the Chern-Simons current is just the dual of the gauge field, the same massless pole also appears in the Chern-Simons correlator, and it's residue determines the topological susceptibility in the large N limit to be

$$\chi_t = \frac{3M^2}{\pi N} + O\left(\frac{1}{N^2}\right) \quad (45)$$

When formulated in terms of the Chern-Simons correlator, 2D CP^{N-1} and 4D QCD have a similar topological charge structure at low momentum. In both cases, the topological susceptibility is just the residue of the massless pole in the Chern-Simons current correlator. The massless Chern-Simons pole embodies the “secret long range order” associated with topology in gauge theory [12]. The physical significance of this massless pole is subtle. Since the CS correlator is not gauge invariant, a $q^2 = 0$ pole does not imply the existence of a massless particle. On the other hand, since the residue of the pole is the gauge invariant topological susceptibility, the pole term in the CS current correlator is in fact gauge invariant and cannot be transformed away. It thus represents a real physical long range correlation which is built into the gauge field by virtue of its topological fluctuations. Nevertheless, in the $q^2 \ll 4M^2$ approximation, the topological charge correlator

$$\tilde{G}(q^2) = \frac{1}{4\pi^2} q^2 \Delta(q^2) \quad (46)$$

is a polynomial in q^2 , so that in coordinate space it collapses to local contact terms. Numerically on the lattice, this leads to a $G(x)$ that is extremely short-range.

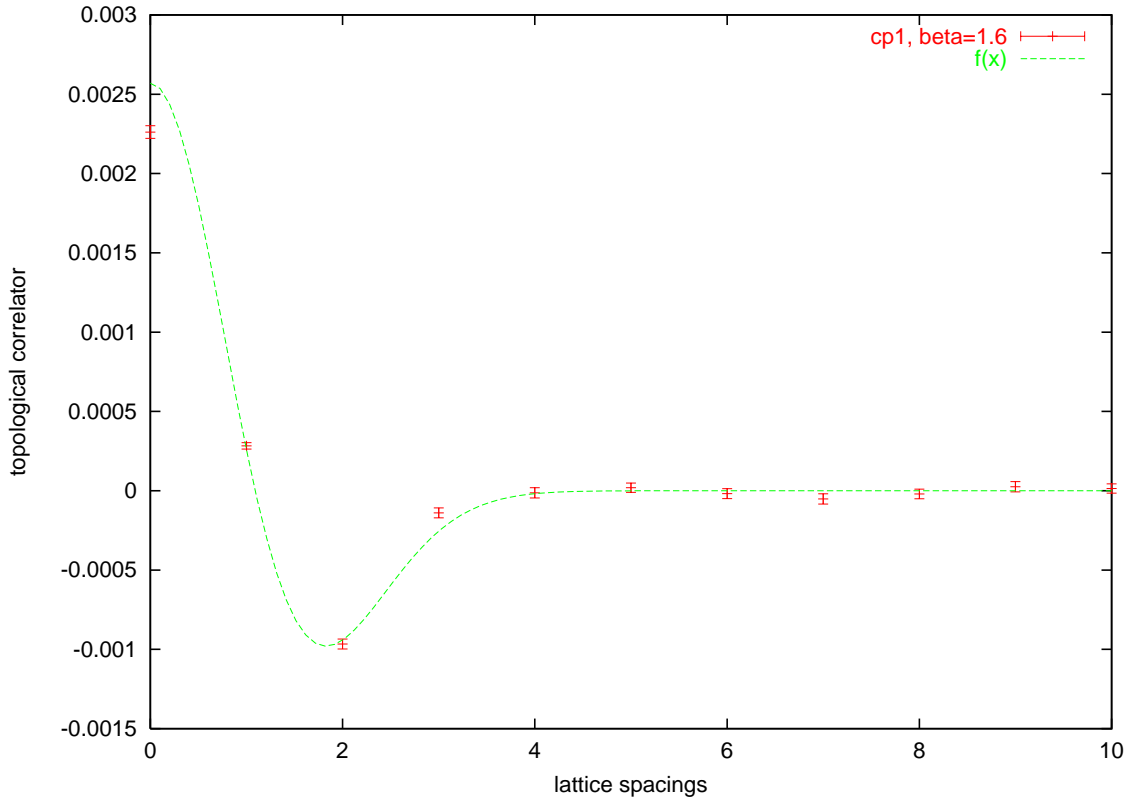


FIG. 9: Pure contact term fit to the two-point topological charge correlator in CP^1

In the remainder of this section, we will discuss the contribution of small instantons to the correlator in the approximation of keeping only the contact terms in $\hat{G}(t)$. In this approximation, the time-dependence of the correlator is simply

$$\hat{G}(t) = -c_1 \delta''(t) + c_2 \delta(t) \quad (47)$$

We note that the numerical calculation of the topological susceptibility from the integral of the lattice correlator[9] involves a large cancellation between the positive part of the correlator at $t = 0$ and 1, and the negative short-range tail from $t = 2$ to $t \approx 4$ or 5. A similar cancellation has been observed in 4D QCD [3]. For the CP^{N-1} models, we find that, as beta is increased, the range of the negative tail remains approximately fixed *in lattice units* as discussed in Section II. This leads us to conclude that the negative tail of the correlator may be treated as part of the contact term, arising from the δ'' term in (47).

Normal scaling behavior for the coefficients c_1 and c_2 would be

$$c_1 \sim \text{const.} \quad (48)$$

$$c_2 \sim \mu^2 \quad (49)$$

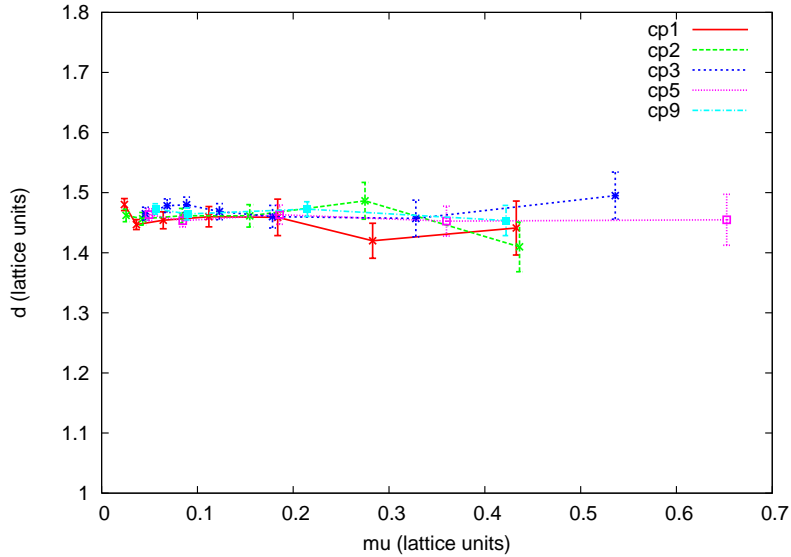
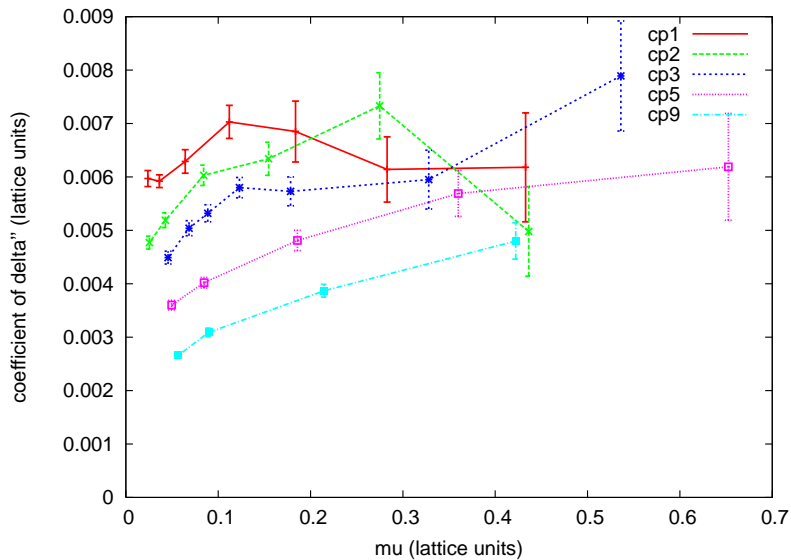
In order to use Eq. (47) as a fitting formula to extract the coefficients of the contact terms from the Monte Carlo data, we employ the following parametrization of a smeared delta function:

$$\delta(t) \rightarrow \frac{1}{d\sqrt{\pi}} e^{-t^2/d^2} \quad (50)$$

The second derivative of this expression also provides a fitting function for the $\delta''(t)$ term in the correlator. We then fit the correlator to a sum of a $\delta(t)$ and a $\delta''(t)$ term. The parameters which are allowed to vary in these fits are c_1 , the coefficient of the δ'' term, and d , the smearing distance. The parameter c_2 is just the susceptibility χ_t , which is computed separately and held fixed in the fits. With these lattice approximations to $\delta(t)$ and $\delta''(t)$, the expression (47) provides a good fit to all of the correlators studied. Fig. 9 shows a typical fit. This plot is for CP^1 at $\beta = 1.6$. The scaling behavior of the smearing parameter d provides a significant test of the pure contact term assumption, Eq. (47). In Fig. 10 we plot the fit values for d as a function of μ for various CP^{N-1} models. In all cases, d approaches a finite value *in lattice units* of $d \approx 1.5$ lattice spacings. This is roughly the same as the measured thickness of domain walls reported in [9]. Thus, the physical range of the correlator goes to zero in the continuum limit. This provides strong numerical support for the assumption that the correlator is well-approximated by contact terms alone. The scaling properties of $c_2 = \chi_t$ for the various CP^{N-1} models have already been discussed. In particular, for CP^1 and CP^2 , c_2 exhibits anomalous scaling properties due to small instantons. In Fig. 11 we have plotted the value of the c_1 coefficient as a function of μ for several CP^{N-1} models. From these results, we conclude that c_1 scales properly (i.e. approaches constant) as a function of μ for all the CP^{N-1} models. Most notably, unlike c_2 , the coefficient c_1 does not appear to receive divergent contributions from small instantons, even for CP^1 and CP^2 . The result that small instantons contribute only to the c_2 coefficient and not to the c_1 coefficient is also expected on theoretical grounds, as we discuss in the next section. The fact that c_1 scales canonically (i.e. approaches a finite constant) in the continuum limit provides further support for the consistency of the pure contact term approximation for the topological charge correlator.

V. HOLOGRAPHIC AND CONFORMAL PROPERTIES OF TOPOLOGICAL CHARGE IN CP^{N-1}

All of these results have a natural interpretation in terms of a two-component picture for topological charge fluctuations in CP^{N-1} models, which we propose and discuss in this Section. To motivate this picture, we first observe that the required negativity of the $\langle q(x)q(0) \rangle$ correlator for

FIG. 10: The parameter d defined in Eq. (50)FIG. 11: β dependence of the OPE coefficient c_1 defined in Eq. (47)

nonzero separation has a fundamental dynamical effect which strongly constrains the types of topological charge fluctuations which can contribute significantly to the vacuum path integral. The way that this constraint is realized in Monte Carlo configurations is by the predominance of topological charge distributions which have a “subdimensional” character, i.e. ones in which coherent regions of topological charge are effectively either zero-dimensional (small instantons) or one-dimensional (Wilson lines). A more unified perspective on both of these types of topological charge excitations can be obtained by considering Witten’s holographic formulation of theta dependence in gauge

theory [5]. In this formulation, the theta term in 4D Yang-Mills arises from compactification of a 5D Chern-Simons term. Similarly, we can interpret the theta term in CP^{N-1} as a compactified 3D Chern-Simons term,

$$\mathcal{L}_{CS} = i\epsilon^{abc} A_a \partial_b A_c \quad (51)$$

Here, a, b, c, \dots run from 1 to 3. Let us denote the original spacetime dimensions by 1 and 2, and the compactified dimension by 3. Then in the limit of small radius of compactification, the Chern-Simons term reduces to a theta term,

$$\mathcal{L}_{CS} \rightarrow i\frac{\theta}{2\pi}\epsilon^{\mu\nu}\partial_\mu A_\nu = i\theta q(x) \quad (52)$$

where $\mu, \nu = 1, 2$, and

$$\theta = \oint A_3 dx_3 \quad (53)$$

From this 3-dimensional framework, a small instanton in CP^1 or CP^2 can be interpreted as a charged particle coupled to the gauge field A_3 which has a world line wrapped around the compact direction in a closed loop, and is pointlike in the 1-2 plane. On the other hand, we may integrate by parts and write,

$$\mathcal{L}_{CS} = -\frac{i}{2\pi}\epsilon_{\mu\nu}(\partial_\mu\theta)A_\nu \equiv J_\nu A_\nu \quad (54)$$

where

$$J_\nu \equiv \frac{1}{2\pi}\epsilon_{\mu\nu}\partial_\mu\theta \quad (55)$$

In this way of writing the CS term, the current J_μ couples to the gauge field in the 1-2 plane. In the limit of small compactification radius, the quantity θ defined by (53) reduces to the constant theta parameter of the 2D theory, but only mod $2\pi k$, where k is an integer which labels a local k-vacuum state. These k-vacua are separated by domain walls, and the current J_μ is an “edge current” which is nonvanishing along these domain walls.

Thus, the 3D Chern-Simons/holographic view of theta dependence in CP^{N-1} models provides a more unified picture of the two dominant types of topological charge excitations in CP^{N-1} models. In 3-dimensional spacetime, both small instantons and the domain walls associated with Wilson line excitations are 0-branes, i.e. particle-like excitations with 1-dimensional world lines. They differ only in the orientation of their world line with respect to the compactified dimension, with small instantons being wrapped around the compact direction localized in the 1-2 plane, and

domain walls being world lines stretched out in some direction in the 1-2 plane. Some further insight into this structure, which also exposes an apparent string/gauge connection, can be gained by considering the 2D CP^{N-1} models in Lorentz gauge, $\partial_\mu A_\mu = 0$. In this gauge, the 2D A_μ field may be written in terms of a single scalar field:

$$A_\mu = \epsilon_{\nu\mu} \partial_\nu \Phi \quad (56)$$

The Chern-Simons current is the gradient of Φ , and the topological charge is its Laplacian,

$$\nabla^2 \Phi(x) = 2\pi q(x) \quad (57)$$

The Monte Carlo results discussed here and in Ref. ([9]) suggest the following idealization: Let us suppose that regions of nonzero topological charge in the vacuum are confined to zero- and one-dimensional submanifolds of two-dimensional spacetime. In this idealized view, spacetime consists mostly of voids in which $q(x) = 0$, with topological charge being confined to either isolated points (small instantons) or to boundaries between voids (domain walls). In the voids $q(x) = 0$, and (57) implies that $\Phi(x_1, x_2)$, within a localized region of spacetime and for a given gauge configuration, is a harmonic function, which can be written in terms of holomorphic and anti-holomorphic conformal fields,

$$\Phi(x_1, x_2) = \phi(z) + \phi(\bar{z}) \quad (58)$$

where $z = x_1 + ix_2$. In this framework, conformal symmetry is broken by the presence of instantons and domain walls in the vacuum, represented respectively by poles and cuts in the analytic structure of $\phi(z)$ configurations contributing to the path integral. The local conformal properties of the gauge field implied by this picture provide some insight into the collapsing of the OPE for the topological charge correlator discussed in Section IV. To illustrate this point, consider the leading OPE term for the CS correlator (22), which is conformally invariant. This vacuum insertion term should be equal to the exact correlator in the absence of conformal symmetry breaking. The second term in (22) is proportional to the (dimensionful) topological susceptibility, and thus arises from the breaking of scale invariance due to the presence of poles and cuts in the analytic structure of $\phi(z)$. In terms of the Lorentz gauge scalar field Φ , the Chern-Simons current is $J_\mu^{CS} = \partial_\mu \Phi$, and the OPE coefficient $C_{1\mu\nu}(x)$ is completely determined up to an overall constant by conformal invariance of the holomorphic and anti-holomorphic terms in the correlator,

$$\langle \partial\phi(z_1) \partial\phi(z_2) \rangle = \frac{\text{const.}}{(z_1 - z_2)^2} \quad (59)$$

and a similar expression for the anti-holomorphic part. The cross-correlators between a holomorphic and an anti-holomorphic field vanish. Using (56) and (58), (59) and the analogous correlator for $\partial_{\bar{z}}\phi(\bar{z})$ completely determine the form of the leading OPE coefficient for the Chern-Simons correlator up to an overall constant,

$$C_{1\mu\nu}(x) = \text{const.} \times \frac{x_\mu x_\nu - \frac{1}{2}x^2\delta_{\mu\nu}}{(x^2)^2} \quad (60)$$

It can now be seen that this OPE coefficient collapses upon differentiation, i.e.

$$\partial_\mu C_{1\mu\nu}(x) = \text{const.} \times \partial_\nu \delta^2(x) \quad (61)$$

This vacuum insertion term produces the $\delta''(t)$ term in the $G(t)$ correlator but does not contribute to χ_t .

In the topological charge correlator, the F^2 insertion term (second term in the OPE (20) or (22)) breaks conformal invariance and provides nonvanishing χ_t . Again, dimensional considerations and Lorentz invariance allow us to write

$$C_{2\mu\nu} = \text{const.} \times \left(\frac{1}{2}\delta_{\mu\nu} \ln x^2 + \frac{x_\mu x_\nu}{x^2} \right) \quad (62)$$

(Here we have dropped an infrared divergent constant $\propto \delta_{\mu\nu} \ln \lambda^2$, where λ is an infrared cutoff mass.) The relative coefficient of the two terms in (62) is determined by the Lorentz gauge condition on the dual A_μ correlator. The long range $\ln x^2$ behavior of the Chern-Simons correlator coming from (62) corresponds to the massless $1/q^2$ pole in the momentum space correlator (43) or (44). Thus, the large x behavior of (62) exhibits the hidden long range order of the theory. Again, the corresponding term in the topological charge correlator collapses to a contact term

$$C_2(x) = -\partial_\mu \partial_\nu C_{2\mu\nu}(x) = \text{const.} \times \delta^2(x) \quad (63)$$

It is this term in the correlator which gives nonzero topological susceptibility.

In Section IV it was shown numerically that small instantons only contribute to the C_2 coefficient and not to the C_1 coefficient in the OPE for the $q(x)$ correlator. We can now present a theoretical argument for this by showing that the contribution of small instantons to the Chern-Simons correlator is of precisely the form (62). The distribution of Chern-Simons current around a small instanton at spacetime point y is given by

$$J_\mu^{CS}(x) = \frac{1}{2\pi} \frac{(x-y)_\mu}{(x-y)^2} \quad (64)$$

Thus, the contribution of an instanton to the correlator $\langle J_\mu^{CS}(x/2)J_\nu^{CS}(-x/2)\rangle$ is proportional to

$$\int \frac{d^2y}{(2\pi)^2} \frac{(y - \frac{1}{2}x)_\mu (y + \frac{1}{2}x)_\nu}{(y - \frac{1}{2}x)^2 (y + \frac{1}{2}x)^2} \equiv I_1 + I_2 \quad (65)$$

where

$$I_1 = \int \frac{d^2y}{(2\pi)^2} \frac{y_\mu y_\nu}{(y - x/2)^2 (y + x/2)^2} \quad (66)$$

and

$$I_2 = -\frac{1}{4}x_\mu x_\nu \int \frac{d^2y}{(2\pi)^2} \frac{1}{(y - x/2)^2 (y + x/2)^2} \quad (67)$$

These integrals are of the same form as the one-loop Feynman integrals for the large- N correlator (although here the integral is over instanton moduli space rather than momentum space). Again, as in (62), we drop infrared divergent constants which do not contribute to the topological charge correlator. This gives

$$I_1 = -\frac{1}{8\pi} \left(\delta_{\mu\nu} - \frac{x_\mu x_\nu}{x^2} \right) (\ln x^2 - 2) \quad (68)$$

and

$$I_2 = -\frac{1}{8\pi} \frac{x_\mu x_\nu}{x^2} \ln x^2 \quad (69)$$

Combining these (and dropping a constant term $\propto \delta_{\mu\nu}$) we get

$$I_1 + I_2 = -\frac{1}{4\pi} \left(\frac{1}{2} \delta_{\mu\nu} \ln x^2 + \frac{x_\mu x_\nu}{x^2} \right) \quad (70)$$

Thus a small instanton gives a contribution to the correlator of precisely the same form as the $C_{2\mu\nu}$ coefficient, (62). We conclude that, within the dilute gas approximation, small instantons contribute only to the c_2 coefficient, in agreement with the numerical results of Section IV.

VI. CONCLUSIONS

Monte Carlo calculations using the overlap Dirac operator to study topological charge structure in CP^{N-1} models have begun to clarify some longstanding issues in these models. The CP^{N-1} models offer an ideal laboratory for studying topological charge in asymptotically free gauge theory, and precise and detailed parallels can be drawn between these models and QCD. Witten's original arguments that instantons in QCD will "melt" due to quantum fluctuations [11] drew heavily on the CP^{N-1} analogy, in particular the absence of instanton effects in the large N solution and

nonzero topological susceptibility at order $1/N$. Lüscher's arguments that topological charge in QCD could be associated with "Wilson bag" surfaces were also supported by the CP^{N-1} analogy, where the corresponding excitation is just the familiar Wilson line. Perhaps the most important simplification in the CP^{N-1} models, relative to QCD, is the fact that in one spatial dimension, a domain wall is a point-like excitation. This allows the success of standard field theory methods such as the large N expansion. The world lines of constituent z -particles which emerge in the large N limit can be identified with domain walls between k -vacua, where the value of $\theta/2\pi$, interpreted as an electric field, changes by one unit of flux.

For the CP^{N-1} models, a value of $N \approx 4$ marks the instanton melting point, i.e. the transition from dominance of $q(x)$ by 0-dimensional instantons to dominance by one-dimensional line-like excitations. From a holographic 3D Chern-Simons viewpoint, the melting of an instanton is actually the unwinding of a Wilson line excitation which was wrapped around the compact dimension. Thus the line-like excitations which are found to dominate the larger N models might be viewed as not only a replacement for the instantons, but in some sense the remnants of melted (unwound) instantons.

The full dynamical implications of small instantons in the CP^1 and CP^2 models remain to be explored. One immediate question is whether these models can have infinite topological susceptibility in the continuum limit and still be consistent field theories. It is hard to imagine a more well-established quantum field theory than the two-dimensional $O(3)$ sigma model, so we would be reluctant to conclude that this model cannot be defined as the continuum limit of a lattice model. What seems more sensible is to regard the topological susceptibility as somewhat analogous to a mass parameter in a field theory with two or more independent mass scales. At least in more benign cases, sending one mass to infinity removes a sector of the theory but leaves the remainder of the theory well-defined. Such an interpretation of infinite topological susceptibility is also suggested by a Witten-Veneziano type argument relating the magnitude of χ_t to the splitting between the singlet and non-singlet mesons. By this argument, $z\bar{z}$ annihilation diagrams, allowed only in the singlet channel, will increase the mass² of the flavor singlet meson by an amount proportional to χ_t . The $O(3)$ sigma model is an exactly solvable model, and its particle spectrum is known to consist of only an isotriplet of mesons, with no isosinglet. From the quark model point of view, this suggests that the mass of the singlet has been shifted upward, if not by an infinite amount, then at least enough to make it unstable. By all indications, the mass shift of the flavor singlet meson is the only singular physical effect of the divergent χ_t , and the resulting theory is in fact well-defined. Direct spectroscopic studies of the singlet channel for various values of N should help to clarify this issue.

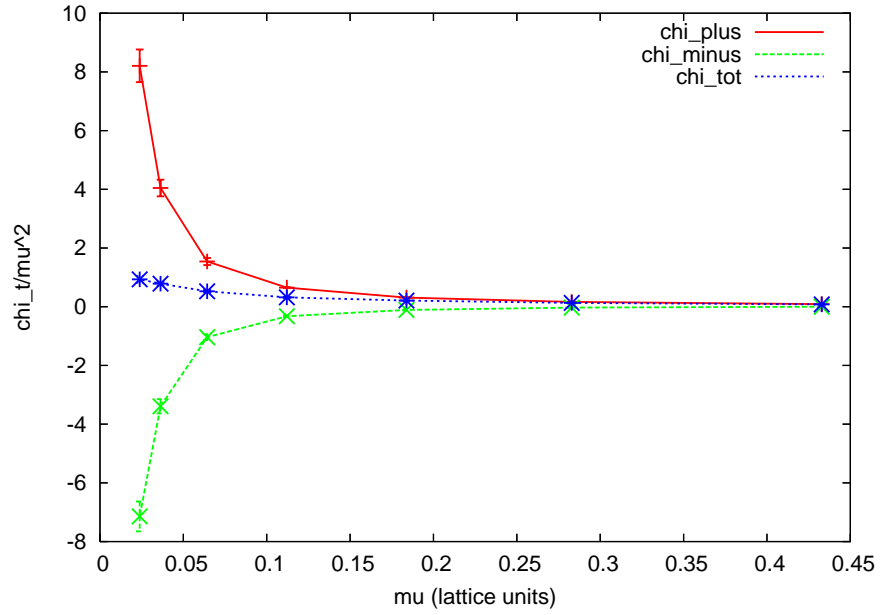
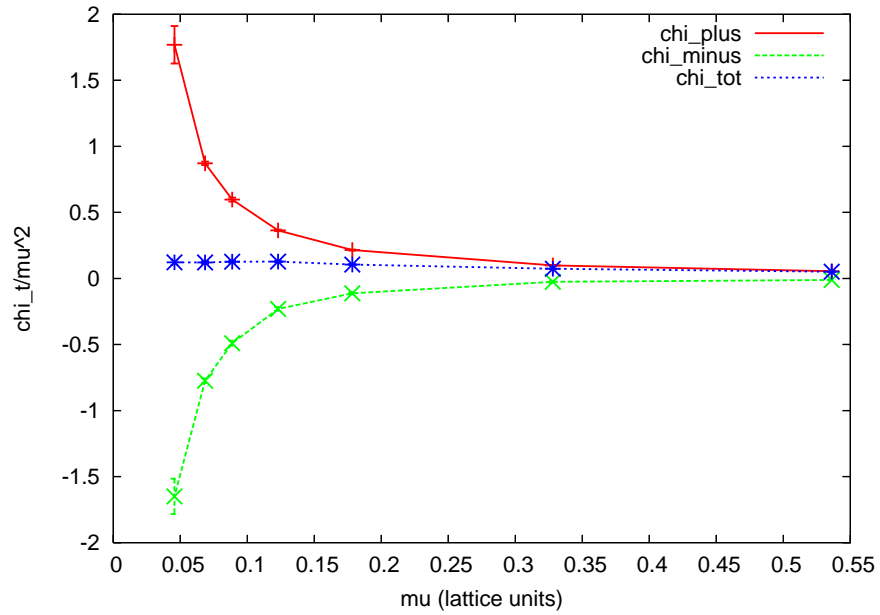
(a) CP^1 (b) CP^3

FIG. 12: Scaling behavior of the positive and negative contributions to the topological susceptibility in CP^1 and CP^3

The lowest dimension operator that couples to the singlet pseudoscalar channel is the topological charge $q(x)$. As we have seen, the two-point correlator for $q(x)$ is dominated by contact terms and has little if any contribution from propagating intermediate states. However, the coupling of $q(x)$ to singlet $z\bar{z}$ states may be suppressed, so it is difficult to even put a lower bound on the singlet mass gap from the $q(x)$ correlator data alone. The study of other operators which couple to the pseudoscalar singlet channel (e.g. smeared $\bar{z}z$ operators) is essential for a complete resolution of this issue.

The fact that the usual scaling $\chi_t \sim \mu^2$ is violated by the contribution of small instantons is not surprising, considering that in the limit of zero lattice spacing, a small instanton consists of a unit of topological charge within a vanishingly small radius, so that the topological charge density is becoming singular in the continuum limit. The topological charge is much more spread out in the case of domain wall excitations and should have a better chance of scaling properly. However, in both CP^{N-1} [9] and in QCD [1], the domain walls are found to be of order lattice spacing in thickness, so that, while they are less singular distributions than the small instantons, they are still not smooth on the lattice spacing scale and would seem to have the potential to cause some problems with the scaling of topological susceptibility. The naive argument that scaling occurs because everything becomes smooth and slowly varying at distances comparable to the lattice spacing is clearly not applicable here. The numerical result that, for CP^3 and higher, topological susceptibility scales like μ^2 and the physical χ_t approaches a finite value in the continuum limit is thus not immediately obvious and probably deserves a deeper explanation. We note that in calculating χ_t the integral under the positive peak from $0 \leq x < 2$ and the integral of the negative tail for $x \geq 2$ cancel with increasing accuracy as beta becomes large, as shown in Fig. 12(a) and 12(b). This figure illustrates that, for the larger N models, the positive and negative contributions to the correlator integral are separately diverging in the continuum limit, but their sum scales properly to a finite topological susceptibility. For the $N > 3$ models, this cancellation reflects the dominance of the $\delta''(t)$ term, whose coefficient scales to a constant, compared to the coefficient of the $\delta(t)$ term, which scales $\propto \mu^2$.

One of our main motivations for undertaking a study of topological charge structure in the CP^{N-1} models was to try to explore the theoretical significance of the recently discovered membrane-like coherent topological charge structure in QCD Monte Carlo configurations [1]. As pointed out by Lüscher [14], one can at least naively estimate the instanton melting point in 4-dimensional $SU(N)$ gauge theory. In Section III we showed that with our lattice formulation of the model, the action of a small instanton was approximately $\epsilon = \frac{N}{2} \times 6.8 \dots$. The critical value

$\epsilon = 4\pi$ gives an instanton melting point of $N_{crit} = 3.7$. It may be possible to increase the small instanton action and thus lower N_{crit} by improvement of the lattice CP^{N-1} action, but the lattice ϵ is bounded above by the continuum instanton action $\epsilon < 2\pi N$, so that any lattice action for the CP^{N-1} model will give

$$N_{crit} > 2 \tag{71}$$

(Thus, in particular, no amount of improvement will completely eliminate small instantons from the CP^1 model.). The lowest possible value of $N_{crit} = 2$ can be estimated within the renormalized continuum theory alone, without reference to a lattice formulation. It corresponds to the “tipping point” in the integral over instanton radius in a semiclassical instanton calculation. This is where the integral changes from being divergent at the small instanton end to being divergent at the large instanton end. (For example, the integral over instanton radius in the CP^1 model goes like $\int d\rho/\rho$.) The analogous integral in 4-dimensional $SU(N)$ gauge theory (using the one-loop beta function) behaves like

$$\int \frac{d\rho}{\rho^5} \rho^{11N/3} \tag{72}$$

which has its tipping point at

$$N_{crit} = \frac{12}{11} \tag{73}$$

By this estimate, the value $N = 3$ for real QCD is comfortably on the large- N side of the critical value, but (73) is only a lower bound on the value of N_{crit} for any particular lattice action, so it is not clear how seriously to take this estimate. The Monte Carlo evidence [1] that membranes, not instantons, dominate the topological charge distribution in QCD adds support for the notion that $N = 3$ QCD is in the large- N regime, above the instanton melting point. As is well-known, the integral over instanton radius in QCD is strongly weighted toward large instantons and must be cut off in an ad hoc way at about $0.3fm$. From the present point of view this is an indication that instantons are unstable toward melting or unwinding. As Lüscher originally argued [12], by periodicity in θ , the vacuum inside a Wilson bag of charge $k = 1$ has the same energy as the $\theta = 0$ vacuum indicating that the confining force between bag walls is completely screened by the appearance of an anti-bag. The analogous process in the CP^{N-1} model is just ordinary string breaking and the vanishing of the area term for integer-charged Wilson loops due to charge screening. With the confining force screened, the bag-antibag dipole layer is free to expand and

produce extended membranes with layers of topological charge of opposite sign juxtaposed, just the type of structure that is seen in the Monte Carlo configurations.

-
- [1] I. Horvath *et al.*, Phys. Rev. D **68**, 114505 (2003) [arXiv:hep-lat/0302009].
 - [2] I. Horvath *et al.*, Phys. Lett. B **612**, 21 (2005) [arXiv:hep-lat/0501025].
 - [3] I. Horvath *et al.*, Phys. Lett. B **617**:49 (2005).
 - [4] C. G. Callan, R. F. Dashen and D. J. Gross, Phys. Rev. D **17**, 2717 (1978). For a review see T. Schafer and E. Shuryak, Rev. Mod. Phys. **70**:323 (1998).
 - [5] E. Witten, Phys. Rev. Lett. **81**, 2862 (1998) [arXiv:hep-th/9807109].
 - [6] For a review, see O. Aharony, S. S. Gubser, J. M. Maldacena, H. Ooguri and Y. Oz, Phys. Rept. **323**, 183 (2000) [arXiv:hep-th/9905111].
 - [7] G. Gabadadze and M. Shifman, Phys. Rev. D **62**:11403 (2000).
 - [8] A. Gorsky, M. Shifman, and A. Yung, Phys. Rev. D **73**: 125011 (2006).
 - [9] S. Ahmad, J. T. Lenaghan and H. B. Thacker, Phys. Rev. D **72**:114511 (2005).
 - [10] H. B. Thacker, PoS LAT2005:324 (2006).
 - [11] E. Witten, Nucl. Phys. B **149**:285 (1979).
 - [12] M. Lüscher, Phys. Lett. B **78**, 465 (1978).
 - [13] B. Berg and M. Lüscher, Nucl. Phys. B **190**, 412 (1981).
 - [14] M. Lüscher, Nucl. Phys. B **200**:61 (1982).
 - [15] P. Hasenfratz, V. Laliena and F. Niedermayer, Phys. Lett. B **427**, 125 (1998) [arXiv:hep-lat/9801021].
 - [16] H. Neuberger, Phys. Rev. Lett. **81**, 4060 (1998) [arXiv:hep-lat/9806025].
 - [17] E. Seiler and I. Stamatescu, MPI-PAE/PTh 10/87, (1987).
 - [18] E. Seiler, Phys. Lett. B **525**, 355 (2002) [arXiv:hep-th/0111125].
 - [19] M. Campostrini and P. Rossi, Phys. Lett. B **272**:305 (1991).